Enhanced surface hydrophobicity by coupling of surface polarity and topography

Nicolas Giovambattista[a,b], Pablo G. Debenedetti[b], and Peter J. Rossky[c,1]

[a]Department of Physics, Brooklyn College of the City University of New York, Brooklyn, NY 11210-2889; [b]Department of Chemical Engineering, Princeton University, Princeton, NJ 08544-5263; and [c]Department of Chemistry and Biochemistry and Institute for Computational Engineering and Sciences, University of Texas, Austin, TX 78712

Edited by Bruce J. Berne, Columbia University, New York, NY, and approved July 7, 2009 (received for review May 17, 2009)

We use atomistic computer simulation to explore the relationship between mesoscopic (liquid drop contact angle) and microscopic (surface atomic polarity) characteristics for water in contact with a model solid surface based on the structure of silica. We vary both the magnitude and direction of the solid surface polarity at the atomic scale and characterize the response of an aqueous interface in terms of the solvent molecular organization and contact angle. We show that when the topography and polarity of the surface act in concert with the asymmetric charge distribution of water, the hydrophobicity varies substantially and, further, can be maximal for a surface with significant polarity. The results suggest that patterning of a surface on several length scales, from atomic to μm lengths, can make important independent contributions to macroscopic hydrophobicity.

computer simulation | contact angle | hydration | surface patterning | wetting

There exists a dichotomy between the usual macroscopic and molecular descriptions of solvation at interfaces. On a macroscopic thermodynamic level, assuming that the surface is homogeneous on the length scale of a test droplet, it is appropriate to focus on the contact angle between the liquid and the solid surface, and the corresponding interfacial tensions (1, 2). On a molecular scale, descriptions typically focus on the character of individual chemical groups that comprise the surface. Surface behavior is then traditionally categorized by chemists and biochemists as polar or nonpolar, and, in the important case when the contacting liquid is water, these descriptions are often equated to the two categories of "hydrophilic" and "hydrophobic." Such designations play a central role in rationalizing a broad range of biochemical phenomena, including protein folding (3), protein-membrane interactions (4), and drug-receptor affinities (5). In the area of protein characterization, it is further common to resolve these two categories of interface chemistry based on an assignment of each amino acid side chain to one of these two categories (4, 6), although there are cases where these designations have been based on individual atomic groups (7). It is, of course, well recognized that the scale of hydrophobicity/hydrophilicity is continuous, and a well-defined division between the two regimes is necessarily arbitrary. It is common practice to identify a macroscopic boundary between hydrophobic and hydrophilic behavior by the convention of a contact angle θ_C of 90°. It has been pointed out, however, that nothing special happens at this particular value of θ_C (8). Evidence revealing the adsorption of water clusters on nominally hydrophobic surfaces shows that such appealing, but simple binary descriptions may be limiting for interpreting atmospheric chemistry, as well (9).

At the same time, the development of "designer" patterned surfaces is an active area (10). In particular, it is widely appreciated that the topography of a surface is important in determining the degree of surface hydrophobicity, with the so-called "lotus effect" (11) being one naturally occurring example. The lotus leaf is "superhydrophobic" ($\theta_C > 150°$) due to a dense distribution of wax-coated protrusions separated on the μm scale, so that the interstitial volumes do not wet and water droplets contact with a substantial area of air. This can be extended synthetically to patterns of holes, spikes, or grooves (12). In fact, considerable technological progress in the development of superhydrophobic surfaces has been made by mimicking natural nanoscale roughness on synthetic surfaces (13, 14, 15). Further, the impact of roughness on hydrophobicity extends down to features that are on the nanometer-scale: Such patterning can induce a substantial increase in hydrophobicity compared with a flat nonpolar surface, although it need not involve the "dry" regions characterizing the lotus effect (16, 17). At the other extreme, superhydrophilic surfaces, with very small contact angles ($\theta_C < 10°$), can be generated by a high density of polar surface groups (18). Hence, controlled microstructure can be used to direct wettability over a wide range (19).

In a hypothetical experiment with a liquid water droplet contacting a macroscopically homogeneous solid surface, as the liquid-solid contact area increased from nano- to microscales, and increasingly averaged over surface heterogeneities, one would expect that alternative measures of hydrophobicity would converge. However, a systematic understanding of the relationship between nanoscale hydration and such macroscale measures for real chemical surfaces remains undeveloped. Understanding the interplay between roughness and chemical character (i.e., molecular polarity) on the nanoscale is one important element toward this goal. Recent work from our labs (20–23) has focused on the contributions of the two elements, surface topography and surface chemistry, at the atomic and nanoscales. We have shown, for example, that nanoscale chemical heterogeneity can produce local perturbations to the hydrophobicity of nanoscale apolar patches (22), and that putative hydrophobic protein surfaces (20) manifest a markedly less hydrophobic signature when the native curved surfaces (24) are flattened. We have also shown for a model chemically detailed surface based on hydroxylated silica (23) that moderate polarity is completely compatible with a hydrophobic contact angle; when the surface polarity of hydroxylated silica is scaled to ≈40% or less of the natural value, the contact angle exceeds 90°. Very recently, Hua, Zangi, and Berne have investigated the wetting of model heterogeneous plates with patterned hydrophobic and hydrophilic sites, and the free energy of interaction between pairs of such surfaces (25). These studies underscore the importance of a quantitative characterization of nanoscale heterogeneity by demonstrating that the length scale characterizing the size of surface hydrophobic patches is a key determinant of wetting behavior and of interaction free energies between surfaces.

Author contributions: N.G., P.G.D., and P.J.R. designed research, performed research, analyzed data, and wrote the paper.

The authors declare no conflict of interest.

This article is a PNAS Direct Submission.

[1]To whom correspondence should be addressed. E-mail: rossky@ices.utexas.edu.

This article contains supporting information online at www.pnas.org/cgi/content/full/0905468106/DCSupplemental.

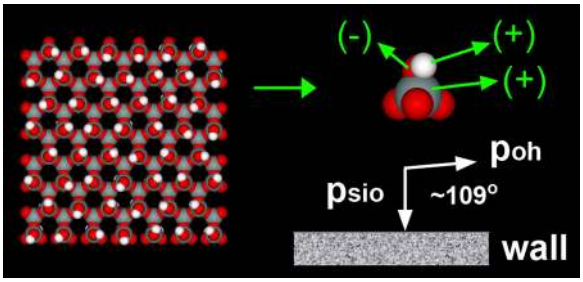

Fig. 1. Structure of the surface of hydroxylated silica that underlies the surface studied here (Si, O, and H atoms are represented by gray, red, and white spheres, respectively). Top-view on *Left*; side view of the surface unit O_3SiO-H at *Upper Right*; schematic of component dipoles on *Lower Right*. We examine hydration of the surface obtained by eliminating the H atom and the OH dipole and then scaling the value of the vertical dipole from this reference value (from SiOH) of p^0 by factors from +2 through zero to −2.

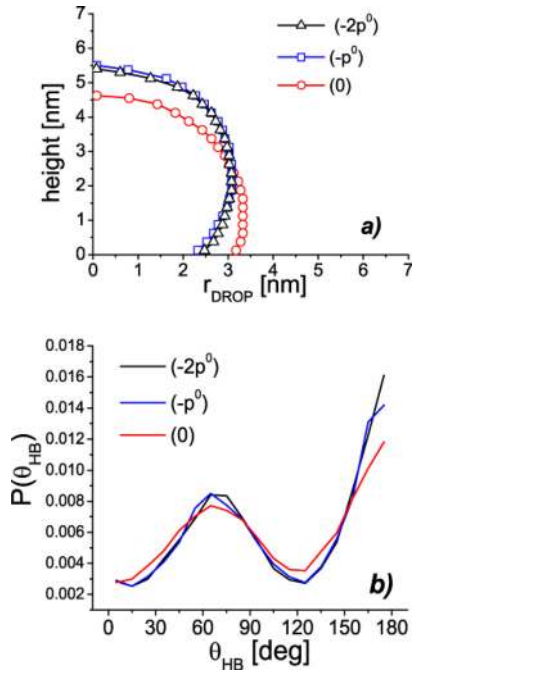

Fig. 2. Response of water to apolar and inverted surface dipole surfaces. (*A*) droplet profiles determining contact angles. (*B*) Probability distribution in the proximal water layer for the four tetrahedral hydrogen bonding directions of a water molecule (OH bond directions and hypothetical lone-pair Oe directions) with respect to the outward pointing surface normal. The proximal layer spans up to a distance 0.233 nm above the outer oxygen atom layer of the surface.

In this article, we present the results of a study of the hydration of a simple, atomically detailed, model interface that includes both atomic-scale roughness and polarity and systematically vary the magnitude and orientation of the polarity. The atomic model used here is based on an earlier model (26) of an idealized crystalline SiO_2 structure (quartz, without any surface reconstruction); here, the atoms are nonpolar except for the surface-exposed oxygen and its bonded nearest-neighbor Si atom, which have equal and opposite partial charges. With this high symmetry and periodic geometry, the solvation structure is readily analyzed. We investigate the roles of the magnitude and orientation of the surface polarity on the solvent energetic and spatial distributions, and on the water contact angle. Since the asymmetric charge distribution in the water molecule itself can substantially influence the relative strength of interaction of water with positive compared with negative charges (27), one cannot a priori predict the influence of polarity reversal on the solvation structure. We find that the response to polarity inversion is, in fact, highly asymmetric.

This article is organized as follows. We first present the essentials of the model system, and then we turn to a detailed analysis of solvent density and orientational response to surface polarity. The results are interpreted in terms of the solid surface structure and the electrostatic forces due to the surface partial charges. The Discussion considers the impact of the results and speculates on the potential implications for real surfaces, which includes the possibility of patterning on multiple length scales. The Methods used are outlined in more detail in the final section.

Model and Primary Observations

In previous work (23), we performed computer simulations of water confined by walls with the structure and chemistry (hydroxylated silica) shown in Fig. 1. We explored the effects on water structure and surface hydrophobicity when the magnitude of the surface polarity was continuously varied (by rescaling the hydroxylated silica model partial charges by a constant k, $0 \le k \le 1$). As explained in ref. 23, the surface polarity is defined by the dipole vectors $\boldsymbol{p}_{\mathbf{SiO}}$ and $\boldsymbol{p}_{\mathbf{OH}}$ associated with each surface SiOH group. In the present article, we examine the impact of polarity orientation using a simpler, more easily visualized, interface model. The surfaces here are also based on plates with the atomic structure of silica, with no hydroxylation, but retain polarity in the surface "Si-O" bond and only in that bond. As a reference value for the polarity $\boldsymbol{p}$, we use the value of $\boldsymbol{p}$ for the SiO bond in SiOH, $\boldsymbol{p}^{\mathbf{0}} = \boldsymbol{p}_{\mathbf{SiO}} = 0.0470\ e\text{-}nm$, for which the partial charges have the values $\pm\ 0.31e$. In addition to the previous results for the hydroxylated surface, we consider the five cases* with a surface SiO dipole $\boldsymbol{p}$ in the range $2\boldsymbol{p}^{\mathbf{0}} \ge \boldsymbol{p} \ge -2\boldsymbol{p}^{\mathbf{0}}$, in increments of $\boldsymbol{p}^{\mathbf{0}}$. The details of the simulations are described in the Methods section.

To see the phenomenon that is the main topic of this report, we start by considering the cases where the surface polarity is inverted from that characteristic of silica. The corresponding water droplet profiles are shown in Fig. 2*A*. Water contact angles θ_C for $\boldsymbol{p} = 0$, $-\boldsymbol{p}^{\mathbf{0}}$, $-2\boldsymbol{p}^{\mathbf{0}}$ are 108°, 127°, and 121°, respectively. A dipole perpendicular to the surface, with the positive charge end pointing into the droplet enhances the surface hydrophobicity even when that dipole moment is substantial ($-2\boldsymbol{p}^{\mathbf{0}}$ corresponds to partial charges of $\pm\ 0.62e$; the H atom partial charge in the SPC/E water model is 0.4238e). From a bulk simulation of water in a slab geometry adjacent to the same surfaces (23), we extract for the proximal layer of water near the surface, the distribution of the four tetrahedral water hydrogen bonding directions, $P(\theta_{HB})$, with respect to the outward pointing surface normal. Fig. 2*B* reveals the characteristic orientational pattern for an extended hydrophobic surface (28) with one HB direction pointing directly into the surface. It is clear that the surfaces with greater contact angle have sharper orientational profiles, in agreement with ref. 23, where $P(\theta_{HB})$ became sharper at $\theta_{HB} = 70°$ and 180° as the surface polarity was decreased toward apolar. In a recent work (29), the contact angle of water in contact with a graphite (apolar) surface in the presence of an external electric field has been studied by simulations with the same water model (SPC/E) as used here. In that work, it was found that the contact angle is sensitive to the magnitude and direction of an external electric

*This is done by re-defining the charges of the SiOH group. For example, when only the SiO dipole component of the SiOH group dipole is left (i.e., $\boldsymbol{p} = \boldsymbol{p}^{\mathbf{0}}$), the charge of the H is fixed to zero, and the O charge is equal to minus the Si charge.

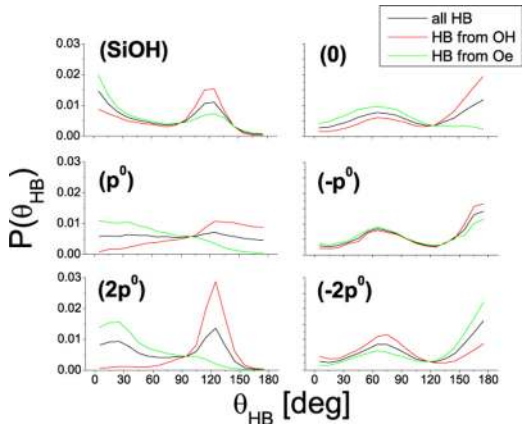

Fig. 3. Probability distribution of hydrogen bond orientations in the proximal water layer, as in Fig. 2*B*, but for the OH bond directions (HB-OH) and hypothetical lone-pair (HB-Oe) directions separately, compared with the sum, for each of the surfaces studied and for the underlying hydroxylated silica surface model (SiOH). Angles are relative to the outward surface normal and the solvent. The proximal layer spans up to a distance $z \leq 0.233$ nm above the outer oxygen atom layer of the surface.

field. However, in ref. 29, the contact angle is largest (for a field aligned perpendicular to the surface) when the external electric field is zero, suggesting that the atomic topography of the present surface plays a role here.

Hydration Analysis

To understand this result more completely, we consider, first, the water molecule orientational distribution in more detail. The hydrogen-bond vector distribution shown in Fig. 3 includes separately the distributions obtained when only the directions associated with water OH bonds and O-lone-electron pair directions (Oe) are used, and we include the distributions obtained for hydroxylated silica (23). For the most polar of the model surfaces (SiOH and $2\boldsymbol{p}^{\mathbf{0}}$), the preference for OH bonds to hydrogen bond to the surface oxygens is clearly shown by the peak at 120°, which also indicates that the water sits in a threefold site between oxygens. For the SiOH, the surface site can be either donor or acceptor, so that the Oe direction behaves similarly to OH, while for the simpler $2\boldsymbol{p}^{\mathbf{0}}$ model surface, the polarities are distinct, with Oe preferring to point outward. It is clear that the $\boldsymbol{p}^{\mathbf{0}}$ surface is simply a weaker version of $2\boldsymbol{p}^{\mathbf{0}}$. When the polarity is reversed, the result is not simply to reverse the roles of each solvent component. The fact that water is asymmetric in its charge distribution, with a localization of the positive partial charge near the H atoms, but a broadly delocalized net negative charge distribution in the "lone-pair" region is well appreciated in the interpretation of ion solvation (27) and the polarization of the water vapor-liquid interface (30, 31). Hence, a lack of symmetry is not completely surprising. What is more notable, however, is the fact that the nonpolar case shows a distinct asymmetry, and it is the $-\boldsymbol{p}^{\mathbf{0}}$ case that manifests the most charge symmetry in the water orientational distribution. It is also this $-\boldsymbol{p}^{\mathbf{0}}$ case that displays the maximum contact angle among the set. We note that examination of the dipole moment orientational profiles (data not shown) reflects the same trends with respect to polarity, with the $-\boldsymbol{p}^{\mathbf{0}}$ case showing the least net dipole polarization in the proximal solvent layer. The water-surface interaction energy (see SI) tracks these results as well, with the $-\boldsymbol{p}^{\mathbf{0}}$ case exhibiting only a small net attraction for the surface, comparable to that for the apolar case, and approximately one-third as negative as in the $+\boldsymbol{p}^{\mathbf{0}}$ case.

We note that Fig. 3 shows that for a wall with the present patterned atomic structure, there is a tendency, in the absence

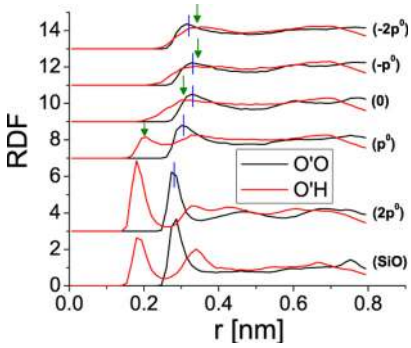

Fig. 4. Radial distribution functions (RDF) of water oxygen O and hydrogen H atoms with respect to surface oxygen (O′) atoms for the surfaces considered. The first peak positions are indicated for H and O in each case as a guide to the eye.

of surface-induced electrostatic fields [panel labeled (0)], for the solvent to orient with a net preference for an OH bond directed at the surface, as reported earlier (23). This is necessarily a result of optimizing the water-water hydrogen bonding around the structured surface, and not to short-ranged steric forces, since the water model is based on an oxygen atom-centered, spherical, nonelectrostatic, short-ranged potential. We will come back to this fact below.

Fig. 4 shows the radial distribution functions (RDFs) between the oxygen atoms of the surface silanol groups (O′) and water H and O atoms. It is clear from the O′O distributions that, consistent with the orientational results, the $2\boldsymbol{p}^{\mathbf{0}}$ surface is nearly as well hydrated as the reference hydroxylated silica. In the $\boldsymbol{p}^{\mathbf{0}}$ case, the hydration is shifted slightly to longer distance and the proximal solvent densities have smaller intensity, indicating a reduced preference, all in accord with expectations. However, reversing the polarity does not simply reverse the orientation of the solvent. In the $-\boldsymbol{p}^{\mathbf{0}}$ case, with the surface "oxygen" now carrying a modest positive charge, the solvent oxygen is shifted to even larger distance, and the hydrogen distribution has an undistinguished character indicative of little orientational preference. Only with the increase of surface polarity to $-2\boldsymbol{p}^{\mathbf{0}}$ does one see the onset of a distinct inversion of solvent orientation and the onset of shortening of the O′O distance due to the attractive polar forces, but even in this case, the hydration is evidently much weaker than for the $+\boldsymbol{p}^{\mathbf{0}}$ case (see Fig. 4 and SI).

Surface Wetting

The results discussed so far largely involve quantities averaged over slabs parallel to the wall. However, these quantities do not give information on how water molecules locate laterally with respect to the surface. Since the surface is structured and not atomically flat, one expects that there will be lateral structural features as well. Specifically, one expects heterogeneity in the local density (see, e.g., ref. 22) that correlates with the structure of the solid surface, i.e., with the location of the SiO_4 groups. To gain insight into the effect of the wall structure on the interfacial water, we follow ref. 22 and evaluate a local density map $n(x, y)$ of relative water density in a thin slab proximal to the surface. Graphical representation, in the form of contour plots, illustrating how water is spatially distributed in the proximal layer is obtained by calculating the time-averaged number of water molecules in a grid of 195 cells laterally distributed over the surface and then converting this digital data into a continuous density distribution $n(x,y)$ by means of Gaussian interpolation (22). In Fig. 5, we present unnormalized density distributions for which relative densities can be directly compared. We use a linear scale in representing the data.

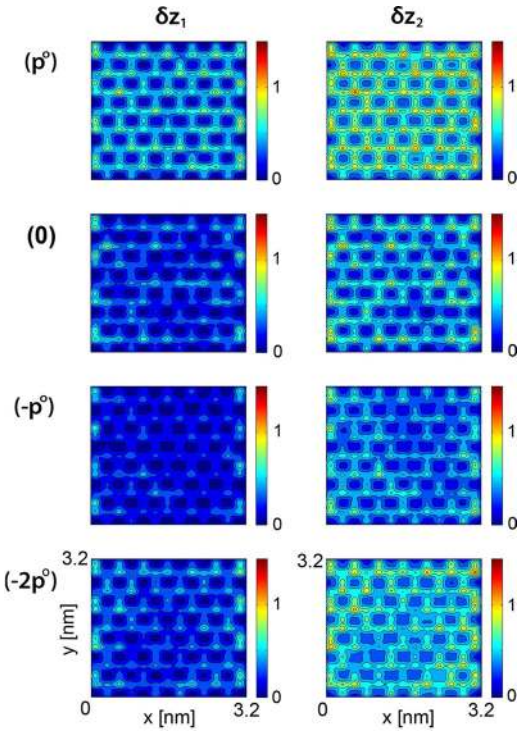

Fig. 5. Density contour maps for water $n(x, y)$ for four surfaces studied at the labeled polarities in a proximal slab of increasing width δz. δz_1: $z \leq 0.233$ nm, *Left* column; δz_2: $z \leq 0.30$ nm, *Right* column, above the oxygen atom layer.

Fig. 5 shows $n(x, y)$ for four surfaces of different polarity, with polarity varying within the column. The first and second columns are the distributions using a slab of width $\delta z = 0.217$ nm, and $\delta z = 0.267$ nm, respectively. The regularly located darkest blue spots in each panel correspond to the sites where the surface oxygen in each SiO_4 group protrudes from the wall. Thus, these sites on the wall are dry by steric exclusion at positions z closest to the wall. These are also the sites where the surface partial charges are located.

Focusing on the variation within each column of Fig. 5, we see, first, that the water closest to the wall preferentially occupies the threefold sites between oxygen atoms in every case, as expected. However, as we move from the $\boldsymbol{p^0}$ surface (first row) to the $-2\boldsymbol{p^0}$ surface (fourth row), we observe that the values of $n(x, y)$ decrease notably in these regions, reaching a minimum for the case of $-\boldsymbol{p^0}$. The effect of inverting the dipole orientation is clearly to destabilize water molecule occupation of the sites between the SiO_4 groups. Comparing $n(x, y)$ for the apolar surface (second row) and the $-\boldsymbol{p^0}$ surface shows that inverting the dipole direction makes the surface slightly drier than completely eliminating surface polarity, in agreement with the enhanced hydrophobicity observed in the contact angle. Increasing the magnitude of this reversed polarity only partially recovers the level of hydration seen for the $+\boldsymbol{p^0}$ case. Comparing the distributions in the two columns of Fig. 5 shows that as we increase the slab width (range of water included), the observations made in the previous paragraph persist, although they become somewhat less pronounced.

Discussion and Conclusions

As noted above, the shape of the patterned atomic surfaces leads, by itself, to a preference for the solvent to orient with a net inward-pointing OH bond at the surface (see Fig. 3). With the introduction of modest positive charges on the outermost atomic layer, the electrostatic forces with the water are not only insufficient to "wet" the threefold sites (that are well solvated for hydroxylated silica and for the $+\boldsymbol{p^0}$ cases), but the solvent is, in fact, mildly repelled from the surface. The overall result is a polar surface that is more hydrophobic than the apolar surface, and one that has a minimal net solvent polarization at the interface.

Another measure of hydrophobicity can be seen when nanoscale hydrophobic surfaces approach closely; liquid water can be expelled from the region between the surfaces (21, 25). In ref. 21, we observed that for two apolar hydrophobic nanoscale plates, with the same atomic structure as those considered here, evaporation indeed takes place at a critical O′-O′ separation between plates of ≈0.67 nm at T = 300 K and zero pressure. One might ask if the "polar hydrophobic" surface exhibits the same loss of wetting, as implied by the other measures reported here. We have carried out corresponding calculations for systems using two identical polar hydrophobic plates, the surface dipole being $-2\boldsymbol{p^0}$ or $-\boldsymbol{p^0}$. In both cases, we observe evaporation at the same O′-O′ separation between plates of ≈0.67 nm (see SI).

Our work suggests that by careful coupling of substrate polarity and topography, it is possible to obtain substantial enhancements of surface hydrophobicity. In the present case, water's tendency to maintain the integrity of its hydrogen bond network results in a localized density depletion in the threefold coordinated sites located between surface oxygen atoms. Substantial enhancement of this depletion results upon imparting mild positive charges onto the protruding sites. If such a surface could be chemically realized, its hydrophobicity could be further enhanced by patterning with micrometer-scale roughness. Such patterning across multiple length scales, ranging from atomic-level control of chemistry to mesoscopic control of topography, could become a powerful tool in the design of surfaces with carefully engineered hydrophobicity/hydrophilicity. Clearly, the present findings are specific to the type of surface considered here. Further work is required before general principles emerge that can guide chemists, biologists, engineers and materials scientists in the rational design of surfaces with controllable water-repelling or water-attracting properties.

Methods

We perform molecular dynamics (MD) simulations of two different systems: (*i*) a water droplet in contact with a periodically infinite wall, and (*ii*) two finite-size nanoscale plates immersed in bulk water. Water molecules are modeled using the SPC/E (32) water model and long range interactions are treated using the Ewald sum technique (33, 34). The temperature is fixed at $T = 300$ K and is controlled using the Berendsen thermostat (35).

To measure water contact angles, we considered a cubic system of side length $L = 13.86$ nm adjacent to a wall of dimensions L x L and of thickness 0.866 nm. The system is periodic along the two long axes of the wall and so is effectively infinite).† Contact angle simulations are run in the *NVT* ensemble. For a given surface, we start the simulations with an equilibrated cubic (edge length 4.66 nm) liquid configuration ($T = 300$ K, $N = 3375$) in contact with the wall. Simulations are run for 500 ps. The cubic water configuration evolves rapidly into a drop-like profile (16, 29, 36–39) and the last part of the simulation (≈300 ps), during which the drop shape is stable, is used to calculate the average drop profile and water contact angle. Details of this analysis method are given in ref. 23. We considered atomistic structured walls, described in detail in refs. 21–23, 26. We considered silica walls composed of four layers of SiO_2, reproducing the structure of the (1.1.1) octahedral face of β-cristobalite (40). The surface not in contact with the droplet is always completely apolar. The Si and O atoms are located in fixed positions. All atoms of the wall interact with the water molecule oxygen atoms via the Lennard-Jones potential. Only the Si and O at the wall surface are charged, and

†The silica nanoscale plates are composed by SiO_4 tetrahedra with dimensions $\Delta x = 0.2475$ nm and $\Delta y = 0.2143$ nm, respectively. With these dimensions, it is not possible to design a silica surface that is (*i*) square, and (*ii*) periodic along both x and y axis. To solve this problem for the simulations of a droplet in contact with an "infinite" wall, we stretched the tetrahedra along the y-axis so $\Delta y \rightarrow \Delta y = 0.2166$ nm. Such a small dilation would not alter any of the previous results of refs. 21–23.

therefore, interact with the water molecule atoms via Coulombic interactions. The wall atom-water interaction parameters are given in ref. 21.

To measure the orientational angle distribution of water next to a given surface and to test the formation of a vapor phase between nanoscale surfaces, we consider a cubic volume containing $N = 3375$ water molecules where periodic boundary conditions apply along the three dimensions. Two finite-size plates of dimensions $3.215 \times 3.217 \times 0.866$ nm^3 are immersed symmetrically about the center of the box, and parallel to each other. The plate chemistry is the same as the chemistry of the wall already described, except that, in this plate geometry case, the outer surfaces of the plates are always hydroxylated. The hydroxyl H atoms on the surface are able to move with fixed bond lengths and bond angles with each H atom of an OH group able to reorient in a circle. The hydration analysis is carried out for a plate (O′-O′) separation of 1.666 nm, so that the two interfacial hydration layers are essentially independent. Simulations are run in the *NPT* ensemble, the pressure being fixed at $P = 0$ GPa using the Berendsen barostat (35). The volume of the system fluctuates with a linear dimension that always exceeds 4.85 nm under the conditions investigated here.

Note Added in Proof. Recently Willard and Chandler (41) have demonstrated the ability of coarse-grained models to capture important characteristics of the interface between water and flat heterogeneous surfaces, including the spatial dependence of the interface width and of water density fluctuations on the patchy substrate.

ACKNOWLEDGMENTS. This work was supported by the National Science Foundation Collaborative Research in Chemistry Grants CHE0404699 and CHE0404695 (P.G.D. and P.J.R.) and R. A. Welch Foundation Grant F-0019 (P.J.R.).

1. de Gennes PG (1985) Wetting: Statics and dynamics. *Rev Mod Phys* 57:827–863.
2. Zisman W (1964) in *Contact Angle, Wettability and Adhesion*, ed Fowkes FM, *Advances in Chemistry Series, 43* (American Chemical Society, Washington, DC), p 1.
3. Nicholls A, Sharp KA, Honig B (1991) Protein folding and association—Insights from the interfacial and thermodynamic properties of hydrocarbons. *Protein Struct Funct Genet* 11:281–296.
4. Wimley WC, White SH (1996) Experimentally determined hydrophobicity scale for proteins at membrane interfaces. *Nat Struct Biol* 3:842–848.
5. VanVeen HW, et al. (1996) Multidrug resistance mediated by a bacterial homolog of the human multidrug transporter MDR1. *Proc Natl Acad Sci USA* 93:10668–10672.
6. Martin-Galiano AJ, Smialowski P, Frishman D (2008) Predicting experimental properties of integral membrane proteins by a naive Bayes approach. *Proteins* 70:1243–1256.
7. Carey C, Cheng Y-K, Rossky PJ (2000) Hydration structure of the α-chymotrypsin substrate binding pocket: The impact of constrained geometry. *Chem Phys* 258:415–425.
8. Granick S, Bae SC (2008) A curious antipathy for water. *Science* 322:1477–1478.
9. Moussa SG, et al. (2009) Experimental and theoretical characterization of adsorbed water on self-assembled monolayers: Understanding the interaction of water with atmospherically relevant surfaces. *J Phys Chem A* 113:2060–2069.
10. See, for example, Cox JK, Eisenberg A, Lennox RB (1999) Patterned surfaces via self-assembly. *Curr Opin Colloid Interface Sci* 4:52–59.
11. Barthlott W, Neinhuis C (1997) The purity of sacred lotus or escape from contamination in biological surfaces. *Planta* 202:1–8.
12. Bico J, Marzolin C, Quere D (1999) Pearl drops. *Europhys Lett* 47:220–226.
13. Feng L, et al. (2008) Petal effect: A superhydrophobic state with high adhesive force. *Langmuir* 24:4114–4119.
14. Roach P, Shirtcliffe NJ, Newton MI (2008) Progess in superhydrophobic surface development. *Soft Matter* 4:224–240.
15. Guo Z, Zhou F, Hao J, Liu W (2005) Stable Biomimetic Super-Hydrophobic Engineering Materials. *J Am Chem Soc* 127:15670–15671.
16. Yang C, Tartaglino U, Persson B N J (2006) Influence of surface roughness on superhydrophobicity. *Phys Rev Lett* 97:116103-1–116104-4.
17. Muller-Plathe F, Pal S, Weiss H, Keller H (2005) Tutorial: Can nanostructuring improve the properties of hydrophobic surfaces? *Soft Materials* 3:21–43.
18. Okabea Y, et al. (2005) Formation of super-hydrophilic surface of hydroxyapatite by ion implantation and plasma treatment. *Surf Coating Tech* 196:303–306.
19. Sun F, Wang G, Jiang L (2003) Stable biomimetic super-hydrophobic engineering materials. *J Am Chem Soc* 125:14996–14997.
20. Giovambattista N, Lopez CF, Rossky PJ, Debenedetti PG (2008) Hydrophobicity of protein surfaces: Separating geometry from chemistry. *Proc Natl Acad Sci USA* 105:2274–2279.
21. Giovambattista N, Rossky PJ, Debenedetti PG (2006) Effect of pressure on the phase behavior and structure of water confined between nanoscale hydrophobic and hydrophilic plates. *Phys Rev E* 73:041604-1–041604-14.
22. Giovambattista N, Debenedetti PG, Rossky PJ (2007) Hydration behavior under confinement by nanoscale surfaces with patterned hydrophobicity and hydrophilicity. *J Phys Chem C* 111:1323–1332.
23. Giovambattista N, Debenedetti PG, Rossky PJ (2007) Effect of surface polarity on water contact angle and interfacial hydration structure. *J Phys Chem B* 111:9581–9587.
24. Hua L, Huang XH, Liu P, Zhou RH, Berne BJ (2007) Nanoscale dewetting transition in protein complex folding. *J Phys Chem B* 111:9069–9077.
25. Hua L, Zangi R, Berne BJ (2009) Hydrophobic interactions and dewetting between plates with hydrophobic and hydrophilic domains. *J Phys Chem C* 113:5244–5253.
26. Lee SH, Rossky PJ (1994) A comparison of the structure and dynamics of liquid water at hydrophobic and hydrophilic surfaces—a molecular dynamics simulation study. *J Chem Phys* 100:3334–3345.
27. Rajamani S, Ghosh T, Garde S (2004) Size dependent ion hydration, its asymmetry, and convergence to macroscopic behavior. *J Chem Phys* 120:4457–4466.
28. Lee CY, McCammon JA, Rossky PJ (1984) The structure of liquid water at an extended hydrophobic surface. *J Chem Phys* 80:4448–4455.
29. Daub CD, Bratko D, Leung K, Luzar (2006) A Electrowetting at the nanoscale. *J Phys Chem C* 111:505–509.
30. Kuo I-F W, Mundy C J (2004) An ab Initio molecular dynamics study of the aqueous liquid-vapor interface. *Science* 303:658–660.
31. Torrie GM, Patey GN (1993) Molecular-solvent model for an electrical double-layer – asymmetric solvent effects. *J Phys Chem* 97:12909–12918.
32. Berendsen HJC, Grigera JR, Straatsma TP (1987) The missing term in effective pair potentials. *J Phys Chem* 91:6269–6271.
33. Toukmaji AY, Board J A Jr (1996) Ewald summation techniques in perspective: A survey. *Comp Phys Comm* 95:73–92.
34. Nymand TM, Linse P (2000) Ewald summation and reaction field methods for potentials with atomic charges, dipoles, and polarizabilities. *J Chem Phys* 112:6152–6160.
35. Berendsen H J C, Postma J P M, van Gunsteren W F, DiNola A, Haak J. R (1984) Molecular dynamics coupling to an external bath. *J Phys Chem* 81:3684–3690.
36. Koishi T, et al. (2004) Nanoscale hydrophobic interaction and nanobubble nucleation. *Phys Rev Lett* 93:185701-1–185701-4.
37. Werder T, Walther JH, Jaffe RL, Halicioglu T, Koumoutsakos P (2003) On the water-carbon interaction for use in molecular dynamics simulations of graphite and carbon nanotubes. *J Phys Chem B* 107:1345–1352.
38. de Ruijter MJ, Blake TD, De Coninck J (1999) Dynamic wetting studied by molecular modeling simulations of droplet spreading. *Langmuir* 15:7836–7847.
39. Shenogina N, Godowat R, Keblinski P, Garde S (2009) How wetting and adhesion affect thermal conductance of a range of hydrophobic to hydrophilic aqueous interfaces. *Phys Rev Lett* 102:156101-1–156101-4.
40. Iler R K (1979) in *The Chemistry of Silica* (Wiley, New York).
41. Willard AP, Chandler D (2009) Coarse-grained modeling of the interface between water and heterogeneous surfaces. *Faraday Discuss* 141:209–220; and discussions therein.